Advances in Nano Research, *Vol. 14, No. 6 (2023) 557-573*
https://doi.org/10.12989/anr.2023.14.6.557

One-step microwave synthesis of surface functionalized carbon fiber fabric by ZnO nanostructures

Ravi S. Rai and Vivek Bajpai*

Department of Mechanical Engineering, Indian Institute of Technology (Indian School of Mines) Dhanbad, Jharkhand, India

(*Received April 15, 2022, Revised October 27, 2022, Accepted November 23, 2023*)

Abstract. The rapid growth of zinc-oxide (ZnO) nanostructures (NSs) on woven carbon fiber (WCF) is reported in this study employing a microwave-aided chemical bath deposition process. The effects of different process parameters such as molar concentration, microwave duration and microwave power on morphologies and growth rate of the ZnO on WCF were studied. Furthermore, an attempt has been taken to study influence of different type of growth solutions on ZnO morphologies and growth rates. The surface functionalization of WCF fabrics is achieved by successful growth of crystalline ZnO on fiber surface in a very short duration through one-step microwave synthesis. The morphological, structural and compositional studies of ZnO-modified WCF are evaluated using field-emission scanning electron microscopy, X-ray diffraction and energy dispersive X-ray spectroscopy respectively. Good amount of zinc and oxygen has been seen in the surface of WCF. The presence of the wurtzite phase of ZnO having crystallite size 30-40 nm calculated using the Debye Scherrer method enhances the surface characteristics of WCF fabrics. The UV-VIS spectroscopy is used to investigate optical properties of ZnO-modified WCF samples by absorbance, transmittance and reflectance spectra. The variation of different parameters such as dielectric constants, optical conductivity, refractive index and extinction coefficient are examined that revealed the enhancement of optical characteristics of carbon fiber for wide applications in optoelectronic devices, carbon fiber composites and photonics.

Keywords: chemical bath deposition; microwave heating; nanostructures; optical characterizations; woven carbon fiber; zinc-oxide

1. Introduction

In the developing era of advance materials, combination of different metal oxide nanostructures along with different base materials having specific properties are combine altogether to fabricate hybrid/composite materials (Liu *et al.* 2022a, Jia *et al.* 2022a). The developed hybrid materials possess tailored properties for diverse applications (Feng *et al.* 2021, Liu *et al.* 2022b). Woven carbon fibers are one of the prominent fibrous material which possesses high strength and light weight required for extensive applications in the field of fiber reinforced polymer composites (Newcomb 2016). Woven carbon fibers are a primary bracing media for polymer composites to enhance the properties of the final composites but single bracing media is not sufficient, thus the concept of secondary reinforcement such as metal oxide nanostructures arises as green field of research (Arani *et al.* 2021, Deka *et al.* 2017). Since very limited work has been done on the growth of nanostructures on woven carbon fiber surface therefore it is required to investigate the advancement of ZnO nano-structured woven carbon fiber materials for varied applications. Out of several metal oxides, zinc oxide (ZnO) is the prominent metal-oxide because of its significant and varied features such as wide energy band of approx. ~3.3 eV at atmospheric condition, piezoelectric nature, optical nature, chemically stable and biocompatible (Mallakpour *et al.* 2021). ZnO is abundantly available non-poisonous metal oxide in nature, which is a cheap semiconductor and can be utilized for a wide assortment of utilization going from sensors, catalysts to solar cells (Ganesan *et al.* 2020). Many ways for blending ZnO into 1-D nanostructures (NSs) with various morphologies, such as nanowires, nanorods, nanoflakes, nanoflowers, nanopallets, and many more superstructures, have recently been published in the literature (Cheng *et al.* 2021, Rai and Bajpai 2021a). The unique properties of ZnO NSs created from synthetic morphology would create undiscovered probabilities for ZnO NSs to be used in a wide range of semiconducting and functional devices, including LEDs, PV cells, solar cells, sophisticated sensors, catalysts, piezoelectric and biological devices (Cortes Herrera *et al.* 2017, Zhang and Xiong, 2015). ZnO nanostructures of can be orchestrated by considerably acknowledged amalgamation techniques such as solvothermal, chemical bath deposition, pyrolysis, sol-gel technique, vapour deposition, microwave assisted technique and others (Baruah and Dutta 2009, Kumar *et al.* 2020). They reveals that due to high amalgamation temperature in most cases, agglomerated NSs formed on the surface which had to be unnecessarily granulated, resulting in little control over molecular shape and size dispersal (Patino-Portela *et al.* 2021). Out of all the strategy for synthesis of ZnO NSs, the aqueous strategy has a several points of interest over other engineered techniques that make chemical bath deposition synthesis as one of the prominent routes for NSs development (Baizaee *et al.* 2018, Kurtinaitiene *et al.* 2016). The chemical bath deposition

*Corresponding author, Ph.D.,
E-mail: vivek@iitism.ac.in

ISSN: 2287-237X (Print), 2287-2388 (Online)

approach is a single-step process that is carried out at low temperature with minimal calcinations and milling, resulting in less agglomeration and better particle distribution (Ma *et al.* 2017, Wang *et al.* 2015). The chemical bath deposition route enables superior purity and phenomenal control over the morphology and size of NSs (Marin-Flores *et al.* 2021, Singh and Azam, 2021). Recently, another method for formation of NSs which is tolerating an impressive proportion of interest of late is the use of microwave warming rather than standard warming which improve the development phenomena, microwave-assisted warming is used for the synthesis of metal-oxide NSs on diverse substrates (Chankaew *et al.* 2019). In this case, the benefits of microwave warming can be used in chemical bath deposition synthesis for annealing sample and precursor solutions (Alshamarti and Omran Alkhayatt, 2020). Because of its various advantages, such as reaction at atmospheric pressure, low response duration, fast warming, low response temperature, uniform heating, and phase immaculateness with better yield, microwave assisted chemical bath deposition amalgamation has gained widespread attention as a new heating route in the development of NSs (Gusmao *et al.* 2021). A rapid combination process called as microwave-aided aqueous course is now being developed for nanostructure production. This is a fast warming method based on microwave dielectric warming of the precursor arrangement, which results in volumetric warming of chemical precursors and solutions. As a result, it is faster, easier, and more energy efficient than traditional conduction heating (Andrade Neto *et al.* 2019).

Several studies have been published on the microwave-assisted wet-chemical development of ZnO nanostructures. However, only a few comprehensive studies on the effects of growth variables on the characteristics of microwave-generated ZnO nanostructures have been conducted. But in case of woven carbon fiber as a substrate, there are very few authors who worked on growth of ZnO on woven carbon fiber however but there is no work related with growth of ZnO nanostructures using microwave assisted chemical bath deposition method on woven carbon fiber surfaces and their optical characterization. Ahmed et al. (Ahmed *et al.* 2014), describe the effect of precursor molar ratio and reaction duration on the shape and aspect ratio of ZnO nanostructures created by microwave aided wet-chemical technique. Radhakrishnan *et al.* (2021), found that changing the microwave power per growth run can vary the morphology of individual ZnO nanostructures from hexagonal cones to faceted hexagonal nanorods to hollow hexagonal nanorods. El-Nahas *et al.* (2021), effectively synthesized ZnO NS with diverse morphologies using a household microwave treatment at 200 Watt power for 15 minutes as well as a minimal amount of capping and complexing agents. Fabrication and characterization of ZnO nanorods upon woven Kevlar fibers by applying low temperature chemical bath deposition process has been achieved by Hazarika *et al.* (2015). Enhancement of energy absorption properties of ZnO embedded WCF composite and their energy transmission under impact loading were discussed by Kong *et al.* (2013). It was found that the grown ZnO nanorods combined with matrix in a crosslinking manner causing high interface properties of final composite. Rai and Bajpai (2021a), concluded that, the nucleation, growth and morphology of ZnO nanostructures on woven carbon fiber by chemical bath deposition route mainly depends on synthesis parameters such as solvent, growth time, precursor concentration, external agitation, seed layer, and pH. Caglar *et al.* (2015), used a microwave-assisted chemical bath deposition approach to study the effects of varying the irradiation period and pH of the precursor solution during the production of ZnO nano-powder. Experiments revealed that the maximum crystal size and crystallinity were attained after 20 minutes of synthesis, and that damage to the crystal structure of ZnO was discovered when the pH value of the growth solution was decreased.

This paper investigates the rapid growth of ZnO nanostructures on woven carbon fiber surface by combining microwave heating with an aqueous process known as the "microwave assisted chemical bath deposition approach". This method allows the generation of ZnO NSs with varied morphologies such as nanowires, hexagonal nanorods, nanoflakes, nanopallets, and nanoflowers by heating WCF samples in different precursor solutions in a household microwave. A probable development phenomenon of various morphologies of ZnO NSs on WCF has been described based on microwave compatibility with materials. Furthermore, study of different process parameters such as molar concentration, microwave duration, microwave power and growth solution were investigated to achieve optimum growth of ZnO NSs on WCF surface. In this study different morphologies of ZnO on WCF strands were grafted by tuning the microwave power, microwave duration and type of precursor solution. The developed ZnO on WCF was characterized to understand their morphologies, size variation, crystallinity and optical behavior. These analyses will provide the basis to implement ZnO embedded WCF to developed advanced nanocomposite materials for optoelectronics and photonics applications. The development of ZnO NSs on WCF surface develops functional groups which may react with the other bracing media and polymer matrix during fabrication of hybrid composites. The current work can implement to develop high performance nanocomposites for industrial applications.

2. Materials and methodology

2.1 Materials

As a substrate material for the synthesis of ZnO NSs, T-300 grade Unmodified WCF with 3000 wires, 0.2mm fabric thickness and 200 GSM size with filament diameter of 7μm was used. Some precursors of analytical-grade are employed in the production of growth solutions and fiber modifications as presented in Table 1. Without any refining, all of the raw ingredients and chemicals were used. Synthesis was carried out on a household microwave with nine power levels and a power output of 1000W at a frequency of 2.45 GHz.

Table 1 List of chemicals used

S. No.	Chemical precursor	Formula	Use
1.	Zinc Acetate dihydrate (ZAD)	$Zn(CH_3COO)_2.2H_2O$	For making growth solution
2.	Ethanol/Acetone	$C_2H_5OH/(CH_3)_2CO$	Cleanser to remove contaminants
3.	Sodium hydroxide	NaOH	For making growth solution
4.	Zinc nitrate hexahydrate (ZNH)	$Zn(NO_3)_2.6H_2O$	For making growth solution
5.	Hexamethyline tetramine (HMTA)	$C_6H_{12}N_4$	To prepare growth solution
6.	De-ionized water (DIW)	H_2O	For making growth solution and rinsing the samples after growth treatment

2.2 Preparation of growth solutions

Microwave aided chemical bath deposition methods were used to produce various morphologies of ZnO NSs. Growth solutions of different molar concentrations were prepared using equimolar (1:1 ratio) solution of ZNH and HMTA in DIW. To prepare 10 mM of growth solution, 2.97 g of ZNH is mixed in 650 ml of DIW using magnetic stirrer operated at 400 rpm and ambient temperature for 45 minutes. Then 1.4 g of HMTA is now added in the prepared solution and stirred for 45 minutes. The resulting solution is now allowed to cool at room temperature and maintained pH of 10-12. Similarly the other concentrations of growth solutions such as 30 mM, 50 mM and 70 mM were prepared. These prepared growth solutions were used for synthesis of ZnO NSs on WCF surface and to study the effect of molar concentrations, microwave duration and microwave power. Furthermore to study the effect of different type of growth solutions on the synthesis of ZnO NSs on WCF, four separate kinds of growth solutions having 30 mM concentration were synthesized and named as A, B, C, and D. To prepare these solutions different set of chemical precursors were mixed in de-ionized water. Solution A was prepared using 2.5 g of ZAD mixed with 500 ml of DIW in a beaker. A magnetic stirrer was used to mix the solution for 45 minutes at 400 rpm at a constant temperature of 50 °C. Similarly, another solution was prepared using 8 gram of sodium hydroxide into 100 ml of DIW. Now gently pour the NaOH solution into the first beaker and vigorously mix for 30 minutes at 400 rpm. Growth solution 'A' is the resultant solution. At a regulated pH of 10-12, the resulting growth solution was allowed to cool to ambient temperature. The precursor mixture (Solution-B) consisted of an equimolar mixture of ZNH and HMTA. Mix 30 mM HMTA in 600 ml DIW for 30 minutes at 300 rpm to make the ZnO precursor mixture (30 mM). The ZNH arrangement was added to the HMTA arrangement, and the resulting mixture was mixed for 30 minutes at atmospheric condition with a pH of 6–8. Similarly, 600 ml of solution-C was made by combining 4.5 gram ZNH, 1.35 gram NaOH, and 13.3 gram HMTA. 2.5 gram of ZAD, 1.35 gram of NaOH, and 13.3 gram of HMTA were mixed in 600 ml of DIW to make solution D. For optimal growth of ZnO NSs onto WCF, all of the resultant solutions should be cooled to room temperature and kept at a pH of 10-13.

2.3 Surface functionalization of WCF

Surface functionalization is a type of fiber modification that comes before the creation of nanostructures on any substrate and is a crucial step. An unaltered form of woven carbon fabric was cut into a square-section of 100 mm × 100 mm dimension to create the sample, and then all of the pieces were cleaned with an acetone-ethanol solution to eliminate dust, dirt, and other impurities that may cling to fiber during manufacture. After dipping the samples in an ethanol-acetone solution for 10 minutes, they were dried in a hot air oven at 90°C for 20 minutes. DIW cleaned the treated WCF many times before drying it in the oven at 90°C for 30 minutes. This phase of surface modification improves the quality of substrate by eliminating foreign impurities and oxides that may be present on the surface and inhibit nanostructure formation (Rai and Bajpai, 2021a). Microwave assisted chemical bath deposition growth technique was employed to produce ZnO NSs from functionalized WCF samples.

2.4 ZnO NSs synthesis on WCF

The prepared growth solution was poured into an oil bath tub in which the dried surface treated WCF samples were dipped then the oil bath tub was placed into a domestic microwave (Samsung-QW71X, 1000 W, 2.45 GHz) for 10 minutes to irradiate the precursor solution and WCF sample. Microwaves travel at the speed of light and consist of two mutually perpendicular electric and magnetic fields which cause linear temperature variation of WCF samples dipped in precursor solution. Since microwave photon energy is moderately low (0.03-0.00003 kcal/mol) and only influences kinetic molecular excitation therefore tetra ammonium zinc complex $[Zn(NH_3)_4]^{2+}$ and OH^- present in the precursor solution started generating ZnO NSs on WCF samples dipped into growth solution, microwave irradiation causes the growth of NSs. After microwave irradiation, the WCF samples were left in the growth solution for 10-15 minutes before being withdrawn and allowed to cool naturally to ambient temperatures. Then DIW is used to rinse the treated WCF and dried the samples in a 70°C oven for 6 hours before storing them at room temperature for 24 hours. The characterization was carried out on the ZnO nanostructured WCF samples that resulted for further study of grown nanostructures. Similarly, ZnO NSs were synthesized under the varying set of experiments

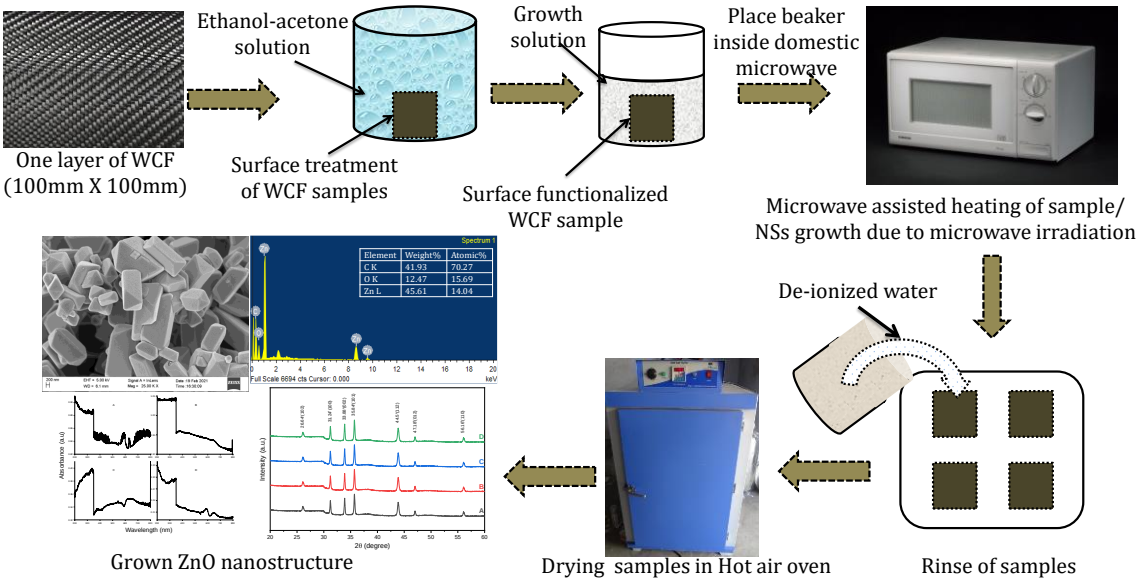

Fig. 1 Stepwise procedure to fabricate ZnO NSs on WCF using microwave-assisted chemical bath deposition

to study the effect of different process parameters such as varying molar concentration (10 mM, 30 mM, 50 mM and 70 mM), microwave duration (5 minutes, 10 minutes, 15 minutes and 20 minutes) and microwave power (250 W, 500 W, 750 W and 1000 W).

The outcomes of these experiments were analyzed and it was found that the optimum growth condition can be developed by varying the type of growth solutions such as solution-A, solution-B, solution-C and solution-D). Furthermore, another set of experiments were performed on varying growth solutions of 30 mM concentration such as A, B, C, and D for the production of ZnO NSs on WCF under microwave irradiation for 10 minutes operated at 1000 W microwave power. The flow chart of synthesis of ZnO NSs on WCF using microwave-aided chemical bath deposition is illustrated in the Fig. 1. Microwave irradiation of the WCF surface produced various distinct morphologies of ZnO under different set of process parameters. According to FESEM data, the sizes of generated ZnO NSs were around 300-2300 nm in longitudinal direction and 200-1100 nm in lateral direction. Following chemical reactions happened during the synthesis of ZnO NSs on WCF using different growth solutions:

$$Zn^{2+} + 4OH^- \leftrightarrow Zn(OH)_4^{2-} \quad (1)$$

$$[Zn(OH)_4]^{2-} \leftrightarrow ZnO_2^{2-} + 2H_2O \quad (2)$$

$$ZnO_2^{2-} + H_2O \leftrightarrow ZnO + 2OH^- \quad (3)$$

$$ZnO + OH^- \leftrightarrow ZnOOH^- \quad (4)$$

$$C_6H_{12}N_4 + 6H_2O \leftrightarrow 6HCHO + 4NH_3 \quad (5)$$

$$NH_3 + H_2O \leftrightarrow NH_4^+ + OH^- \quad (6)$$

$$2OH^- + Zn^{2+} \leftrightarrow ZnO + H_2O \quad (7)$$

2.5 Characterizations

FESEM model-Supra 55 (make-Carl Zeiss, Germany) was used to characterize the generated morphologies and growth structure of ZnO NSs on WCF at various magnifications. FESEM results were also used to examine the size and morphology of the growing NSs. The presence of ZnO on WCF strands was investigated using EDS technique combined with FESEM. The absorption graphs of as generated ZnO NSs on WCF were investigated using UV-vis spectroscopy (model-Agilent Cary 5000) with attachments of an integrating sphere, and study of their optical nature at room temperature were assessed using tauc's plot method. Using wide-angle XRD automated with guidance software (SmartLab Studio II) of Rigaku Smartlab using Cu-K_α radiation imaging, the crystalline structure of the grown morphologies of ZnO on WCF was examined.

3. Results and discussion

3.1 Morphological characterization of as grown ZnO NSs on WCF

3.1.1 Influence of varying molar concentration

The surface morphology of all of the ZnO nano-structures grown on the woven carbon fiber fabrics was directly observed by FESEM. To investigate the influence of the molar concentrations of precursor chemical such as ZNH and HMTA on the growth and morphology of the ZnO nanostructures, a set of experiments was performed. The attachment of ZnO nanostructures may be seen on the surface of the woven carbon fibers as shown in Fig. 2. It was found that the concentrations of zinc nitrate hexahydrate and HMTA had a great influence on the size and structure of the grown nanostructures. At low zinc nitrate hexahydrate and HMTA concentration of 10 mM (Fig. 2a), small ZnO nanorods were found on the surface of

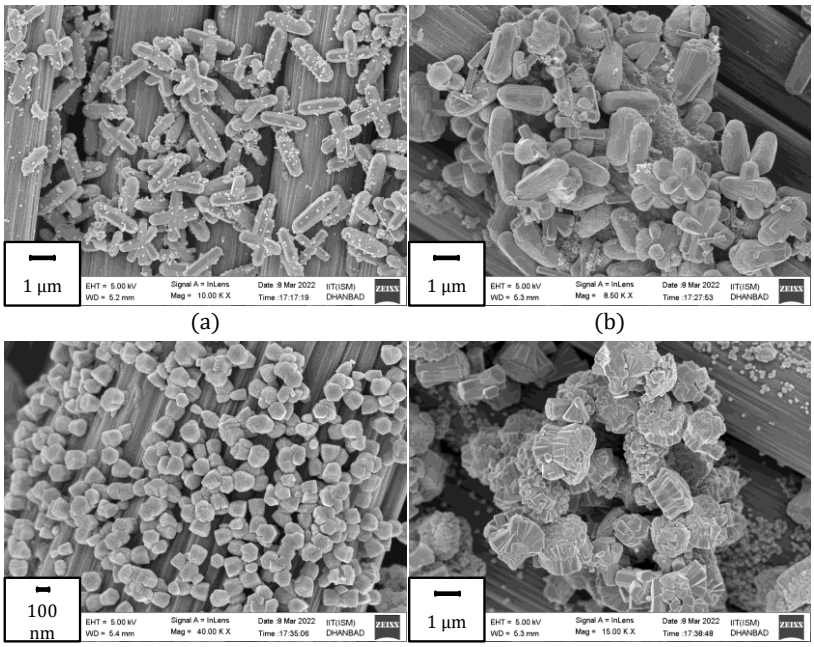

Fig. 2 FESEM results of as grown ZnO NSs on WCF by microwave heating under varying molar concentration (a) 10 mM (b) 30 mM (c) 50 mM and (d) 70 mM

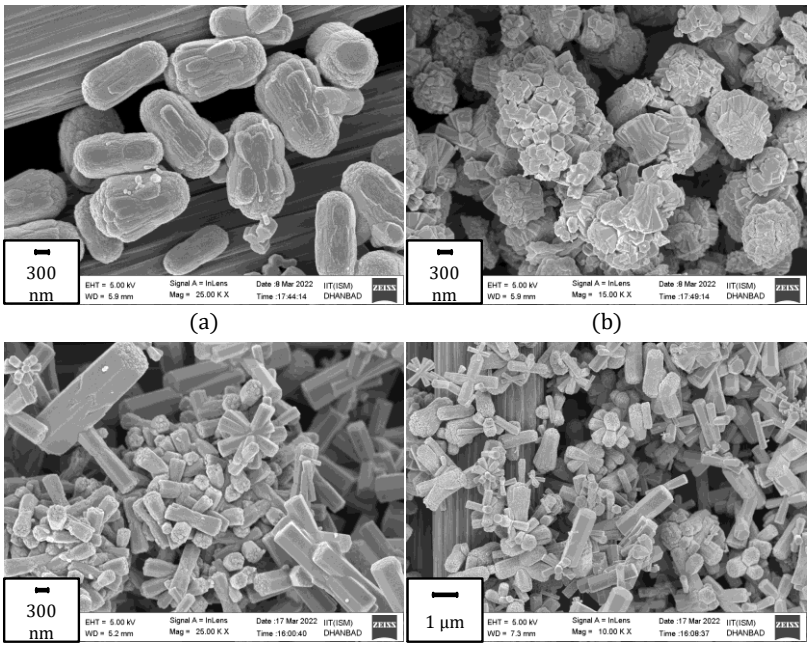

Fig. 3 FESEM results of as grown ZnO NSs on WCF by microwave heating under different microwave duration (a) 5 minutes (b) 10 minutes (c) 15 minutes and (d) 20 minutes

the carbon fiber, but the quantity of nanorods coated on the carbon fiber surface is very less. Furthermore, there are some tiny ZnO crystals were sparsely coated upon large nanorods and fiber surface. A non-uniform and discontinuous layer of grown ZnO nanorods can be seen on all of the samples synthesized at different molar concentrations using the microwave-aided chemical bath deposition except for the sample with a concentration of 50 mM (Fig. 2c).

It is clear that the molar concentration of the growth solution plays a vital role in developing different shape and size of the ZnO nanostructures (Cheng *et al.* 2019). However the variations of molar concentration for growth of ZnO nanostructures on WCF using microwave heating do not developed well distributed nanostructures bonded with carbon fiber surface. Although the ZnO nanorods were grown at a higher concentration (i.e., 30 mM, 50 mM, 70 mM), thicker nanorods were obtained compared to the

lower concentrations. The higher concentration led to the supersaturation and formation of many small nuclei, which results in fast nucleation and a slow growth rate. Consequently, this will retard the growth rate of the (0001) plane and will make the ZnO nanorods thicker and twinned (Fig. 2d) (Edalati *et al.* 2016).

3.1.2 Influence of microwave heating duration

Fig. 3 illustrates the FESEM micrographs of the as-prepared nanorods grown on the ZnO seeded woven carbon fibers after solution based microwave irradiation reaction at different reaction times. It can be clearly seen that the carbon fibers are partially covered with non-uniform ZnO nanorods at lower microwave duration. However the uniformity and density of grown ZnO nanorods are increases as the microwave duration increases and carbon fiber fabric completely covered with a uniform and dense film of ZnO nanorods. The as-prepared ZnO nanostructures were non-uniform hexagonal nanorods with an axial length of 1000-1500 nm and a diameter of 300-500 nm under varying microwave duration (Fig. 3). As the microwave treatment time varies, the shape of nanorods started changing due to twinning of nanorods into flower shape structure. However, the well distributed nanoflower structures were developed at 10 minutes of treatment due to twinning of nanorods into a bunch a flower (Fig. 3b). The length and diameter of developed nanostructures increased with an increase in the reaction time. For instance, the length and diameter increased from 1000 to 1500 nm and 300 nm to 500 nm, respectively, when the reaction time increased from 5 to 20 minutes. Therefore, the reaction time is also an important factor for controlling the size of the nanorods (Rai and Bajpai 2021a).

3.1.3 Influence of microwave power

The effects of microwave power on the growth rate of the ZnO nanostructures were also studied. The microwave power was found to have a great influence on both the axial and lateral growth rates of the nanorods. The microwave power level was found to be proportional to the growth rate of the nanorods, mainly due to the rapid heating of the precursors to its crystallization temperature and quick dissolution of the precipitated hydroxides (Kim *et al.* 2011). It was observed that longer and thicker nanorods may be obtained at higher microwave power levels. Figure 4 shows the FESEM images of as-grown nanorods at different microwave power levels (250 W, 500 W, 750W and 1000 W) for 10 min. A homogenous and continuous film of ZnO nanorods may be seen on the WCF. The hexagonal ZnO nanorods grown at a high microwave power (1000 W) had a greater diameter (300 nm) and length (600 nm) than nanorods grown at 250 W, 500 W and 750 W (Fig. 4a-c). An increase in the microwave power causes the rapid heating of the solution, which enhances the nucleation and growth of the ZnO crystals (Ul Hassan Sarwar Rana *et al.* 2016). The well distributed nanorods of hexagonal cross-section were developed at microwave power of 1000 W for 10 minutes of treatment in 30 mM of reaction mixture as illustrated in Fig. 4d. Therefore, rapid growth of longer and thicker nanorods may be achieved by increasing the microwave power. It may be concluded that the microwave power has a great influence on enhancing the dimensions of the nanorods. The above discussion indicated that a ZnO nanorod film may be successfully prepared on the WCFs.

The size and morphology of the as-prepared nanorods may be controlled by changing the salt concentrations, reaction time and microwave power levels. Therefore, we may conclude that an increase in the concentration of zinc nitrate hexahydrate/HMTA induces changes in the kinetics of nucleation and growth, which may result in a change in the size and density of the ZnO nanorods on the fiber surfaces. Similarly, the reaction time and microwave power also had a great effect on the size and density of the ZnO nanorods. In particular, these parameters influenced the growth rate of the nanorods along different planes resulting in varying sizes of ZnO nanorods. Finally, a controlled and uniform film of ZnO nanorods of the desired shape and size may be developed under optimized parameters. The developed nanostructures under varying experimental conditions such as solution concentration, microwave duration and microwave power are discussed in this work. The development of ZnO nanostructures on the carbon fiber fabric in one-step solution based synthesis is a challenging task because it requires seeding of WCF in a seed solution which produces ZnO nucleation (Hazarika *et al.* 2015). Since some of the developed nanostructures are not well distributed and non-uniform in shape and size, therefore an attempt has been taken to study the effect of different type of growth solution for the development of well distributed ZnO nanostructures on woven carbon fiber fabric. Four different kind of growth solution named as A, B, C and D having 30 mM concentration were prepared using different precursor chemicals in deionized water. These solutions were used to synthesize ZnO nanostructures on carbon fiber fabric.

3.1.4 Influence of variety of growth solution

In the current work the effects of different process parameters such as molar concentration, microwave duration and microwave power on the growth rate of the ZnO nanostructures on carbon fiber fabric were studied. These process parameters were found to have a great influence on morphologies and growth rates of the ZnO nanorods. Furthermore, it is required to study the impact of different kind of growth solutions on morphologies and growth rates of the ZnO nanorods. Four different kind of growth solutions such as A, B, C and D having 30 mM concentration were prepared using precursor chemicals such as ZAD, ZNH, HMTA and NaOH in deionized water. The prepared growth solutions of 30 mM concentration were used to synthesize ZnO nanorods on carbon fiber fabric using solution based microwave irradiation reaction at microwave power of 1000 W for 10 minutes. The grown morphologies and their growth structure of ZnO NSs on WCF by microwave aided chemical bath deposition method under four distinct growth solutions prepared with different set of precursor chemicals are represented by FESEM micrographs. As shown in Fig. 5, different solutions exhibit varied morphologies of ZnO NSs on the strands of carbon fibers, such as nanopetals, nanospheres, nanoflowers, and

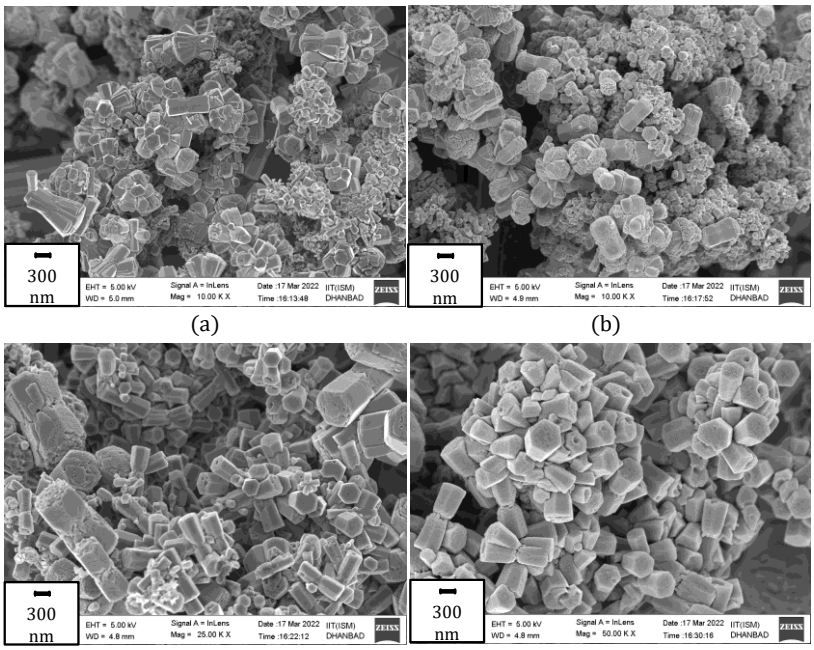

Fig. 4 FESEM results of as grown ZnO NSs on WCF by microwave heating under different microwave power (a) 250 W (b) 500 W (c) 750 W and (d) 1000 W

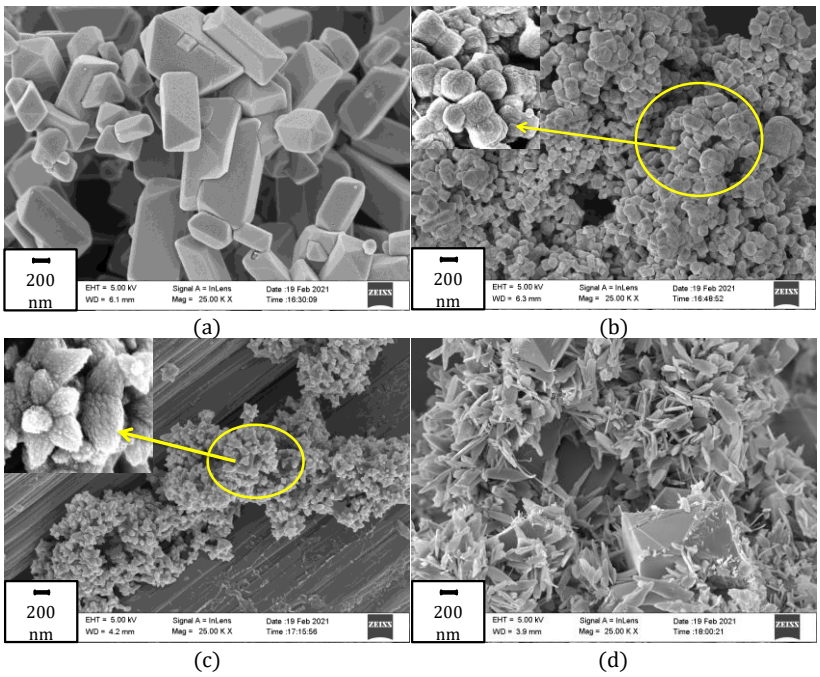

Fig. 5 FESEM results of as grown ZnO NSs on WCF by microwave irradiation under different precursor solutions (a) nanopetals (b) twinned nanospheres (c) nanoflowers and (d) nanoflakes

nanoflakes. The grown nanostructures have an uneven shape, which could be due to post heating at 70 °C for 6 hours in a hot air oven (Kumar and Kanjilal 2018).

The impact of microwave treatment on the precursor chemicals and polar groups present on the WCF surface is the growth mechanism of ZnO NSs on WCF via microwave based chemical bath deposition process. Due to exposure of WCF samples to the electric field during microwave irradiation, precursor chemicals such as ZAD and ZNH in the solution began breaking down into ZnO nuclei, which started acting like dipoles in the precursor solution. After that, under the influence of microwave power of 1000 W, the generated nuclei began polarizing and aggregating to produce ZnO nanostructures on the WCF surface for the duration determined for each sample. ZnO NSs with different morphologies and different dimensions with smooth surfaces were produced because of post heating of samples at 70 °C for 6 hours in a hot air oven. The blossom shaped ZnO NSs were developed on WCF when the microwave power is exposed to the samples for 10 minutes

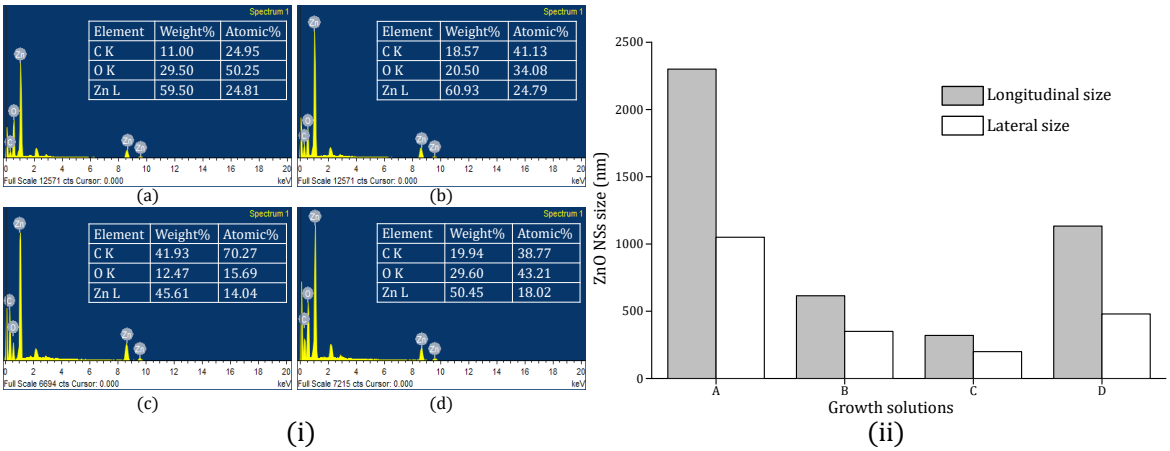

Fig. 6 (i) EDS spectra and (ii) Size distribution of ZnO NSs under different precursor solutions

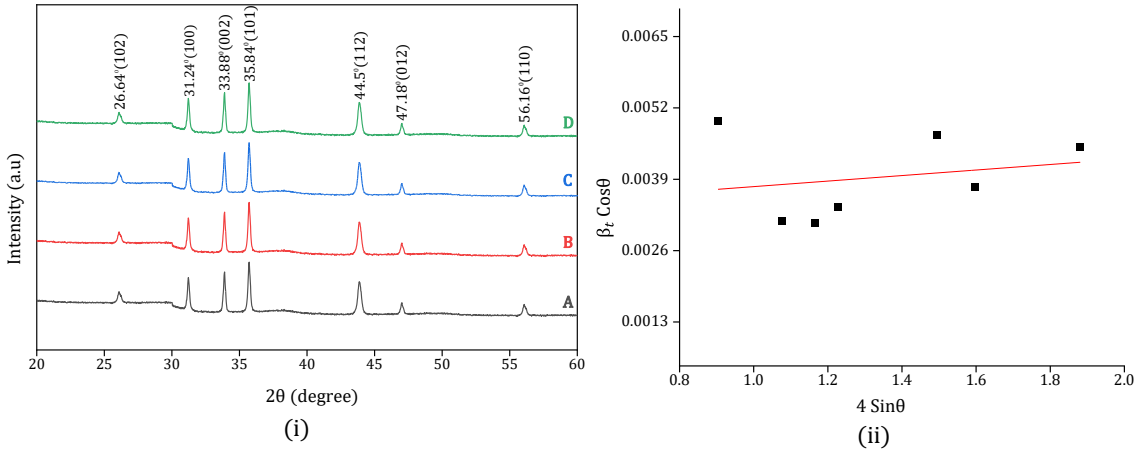

Fig. 7 (i) XRD spectra and (ii) Williamson Hall graph of as grown ZnO NSs on WCF sample

in solution C. The amalgamation of ZNH and HMTA with NaOH caused the flower shape to grow with nine petals as depicted in the inset of Fig. 5(c). While processing WCF in solution D, where the presence of ZAD generates ZnO nuclei, ZnO nanoflakes were generated. Some of the nanoflakes were destroyed due to 10 minutes of microwave irradiation and subsequent heating during post-annealing process. FESEM micrographs were used to calculate the dimensions of the produced ZnO NSs. Different morphologies have different sizes of the NSs mainly in longitudinal and lateral direction as shown in Fig. 6 (ii). Nanopetals and nanoflakes have large longitudinal and lateral sizes, but the overall surface area of nanoflowers and twinned nanoshpheres is substantial, which will improve the surface properties of the final ZnO/WCF samples. The FESEM images confirmed that the ZnO grown on WCF has a variety of morphologies and emerges from the distinct cross-sections of the NSs. EDS spectra indicated the growth of ZnO NSs on WCF surface with weight percentages of Zn and O as shown in Fig. 6(i). It was found that the growth of NSs on WCF is in good quantity with a weight percentage range of 45-62 % of Zn and 12-30% of O. XRD and UV-VIS spectra analysis were used to further investigate the produced ZnO. The EDS spectra analysis demonstrated that the produced ZnO NSs have excellent purity and contain no impurities.

3.2 Structural characterization of grown ZnO NSs

Fig. 7 (i) shows the XRD spectra of as-grown ZnO NSs on WCF fibers, such as nanopetals, twinned nanospheres, nanoflowers, and nanoflakes. The results of XRD peak analysis confirmed that the developed ZnO NSs have a high purity wurtzite phase of ZnO and possess hexagonal crystal system having space group "P 63 m c", space group number-186, a=b=3.2530 A°, α = β = 90°, γ = 120°, cell volume- 47.72 × 10^6 pm^3 and density = 5.66 g/cm^3, JCPDS card no. 96-900-4180). Crystallite sizes of the ZnO NSs were deduced from the XRD peaks using the FWHM of high intensity peak using the Debye Scherrer relation. In this method, the effects of peak broadening of the XRD spectra due to instrumental errors and inhomogeneous strain were not considered. In order to calculate crystallite size (D) and strain (ε) of the synthesized ZnO NSs on WCF, Williamson-Hall (W-H plot) technique was applied by calculating FWHM.

The overall broadening of XRD peaks is the sum of broadening due to crystallite size and broadening due to strain (Caglar *et al.* 2009, Zhao *et al.* 2022). That is,

$$\beta_t = \beta_D + \beta_\varepsilon \quad (8)$$

And the Scherrer formula is,

Table 2 Growth conditions and properties of as grown ZnO NSs on WCF

ZnO/WCF samples	Growth solution	Developed morphology	Microwave duration (minutes)	Crystallite size D_{101} (nm)	Energy level (E_g~eV)
A	A	Nanopetals	10	~38	~3.358
B	B	Twinned-nanospheres	10	~40	~3.29
C	C	Nanoflowers	10	~43	~3.18
D	D	Nanoflakes	10	~32	~3.32

Table 3 Details of texture coefficient of ZnO/WCF samples

Sample	Morphology of ZnO NSs	$T_{c(1\,0\,2)}$	$T_{c(1\,0\,0)}$	$T_{c(0\,0\,2)}$	$T_{c(1\,0\,1)}$	$T_{c(1\,1\,2)}$	$T_{c(0\,1\,2)}$	$T_{c(1\,1\,0)}$
A	Nanopetals	1.21	1.06	1.054	2.35	0.78	1.02	1.24
B	Twinned- nanospheres	1.14	0.97	1.18	2.42	0.92	0.91	0.97
C	Nanoflowers	1.2	1.18	1.23	2.78	0.98	1.06	1.13
D	Nanoflakes	1.01	0.96	1.04	2.26	0.88	0.91	0.96

$$D = \frac{K\lambda}{\beta_D cos\theta} \tag{9}$$

where, K is the shape factor which is equal to 0.9, is the wavelength of X-ray source which is equal to 0.15406 nm, θ (in radian) is the location of peaks and D is the size of grown crystals. The overall broadening of XRD peak may be written as:

$$\beta_t = \frac{K\lambda}{Dcos\theta} + 4\,\varepsilon\, tan\theta \tag{10}$$

Eq. (3) can be written as,

$$\beta_t cos\theta = \varepsilon\,(4\,sin\theta) + \frac{K\lambda}{D} \tag{11}$$

This statement is equivalent to a straight line equation, therefore the W-H graph is essentially a straight line drawn with (4 sinθ) on the x-axis and (β_t cosθ) on the y-axis, as seen in Fig. 7 (ii). The slope of the line will give the amount of strain "ε" and the y-intercept will give the value of crystal size. The computed value of the strain is 5.03698×10^{-4} and the crystallite size is $42.53\,nm$. The observed value of the crystallite size using Scherrer formula for all XRD peaks of ZnO NSs is found to be in the range of 30-40 nm and the analogous value of D corresponding to the high intensity peak (101) of all the samples was observed to be in the range of 32-43 nm as illustrated in the Table 2.

The expression to calculate the texture coefficient $T_{c(h\,k\,l)}$ which will provide the basis to deduce the preferred orientation of crystal growth and their orientation in the (h k l) plane is defined as (Kothari and Chaudhuri 2011):

$$T_{c(h\,k\,l)} = \left(\frac{I_{(h\,k\,l)}}{I_{0(h\,k\,l)}}\right) \Big/ \left[\frac{1}{n}\sum \frac{I_{(h\,k\,l)}}{I_{0(h\,k\,l)}}\right] \tag{12}$$

where, $I_{(h\,k\,l)}$ is the calculated XRD intensity corresponding to (h k l) plane derived from the XRD data, $I_{0(h\,k\,l)}$ is reference data of XRD peak intensities from (JCPDS card no. 96-900-4180) and n is the total number of XRD peaks. The texture coefficients ($T_{c(h\,k\,l)}$) of the as grown ZnO NSs on WCF are tabulated in the Table 3. If the value of $T_{c(h\,k\,l)}$ is more than one then there is affluence of grain in the corresponding plane but if the value equal to one then it shows random orientation of crystals. It can be observed that the largest value of $T_{c(h\,k\,l)}$ lies in the plane (101) for each sample but sample C (nanoflowers morphology) has the highest value of texture coefficient because of the larger surface area of nanoflowers as mentioned in Table 3. Finally it can be concluded that the preferred orientation for the crystal growth of ZnO NSs is along the (1 0 1) plane which is largest for sample-C.

3.3 Optical characterization of ZnO NSs grown on WCF

The optical properties of produced ZnO NSs on WCF were investigated using a UV-vis spectrophotometer with a wavelength range of 200-800 nm (visible range). UV-vis analysis of samples was analyzed by optical absorbance, optical transmittance and optical reflectance spectrum in the visible range as illustrated in Fig. 8, Fig. 9 and Fig. 10 respectively. At a particular wavelength sample illuminates due to the absorption of that radiation and at the remaining wavelength no absorption will occur. In the same way transmittance and reflectance will be seen while transmitting and reflecting that radiation at a particular wavelength. ZnO include a large direct energy band and large exciton energy at atmospheric conditions (60 meV). From Fig. 8, the strong absorption occurred near ~353 nm wavelength for all the samples that exhibit presence of ZnO because pure ZnO has band gap (Eg=3.37eV) in the wavelength range of ~ 360nm. In Fig. 8(a), the graph shows that the absorbance varies nonlinearly, however there is a sharp decline in absorbance at wavelengths near ~350-355 nm, which is due to optical conversions occurring at the energy level of the ZnO nanopetal morphology. In Fig. 8(b and d) there is a decrement in the absorption value just after the wavelength of ~ 350-355 nm and small variation near the wavelength of 650 nm which may be due to oxygen

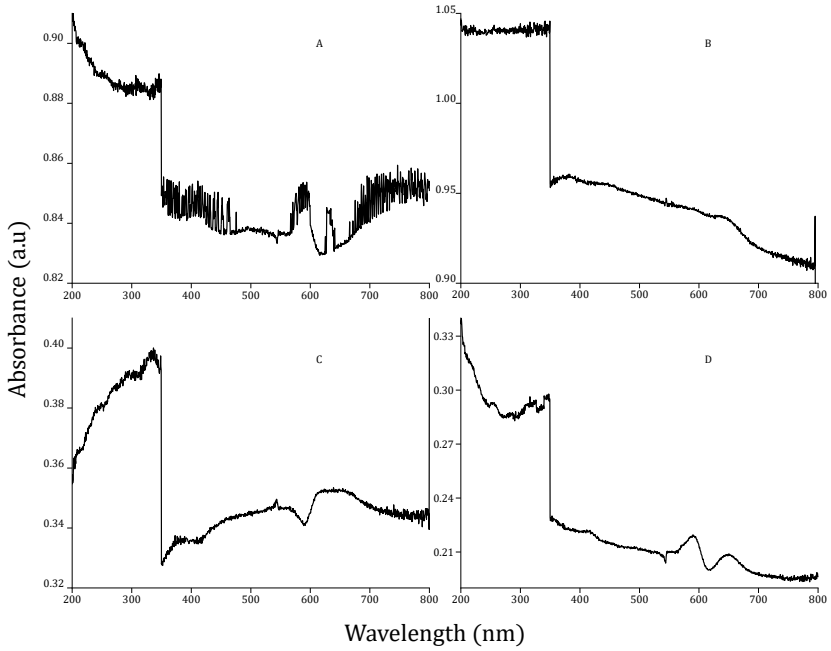

Fig. 8 Optical absorbance of ZnO NSs grown on WCF

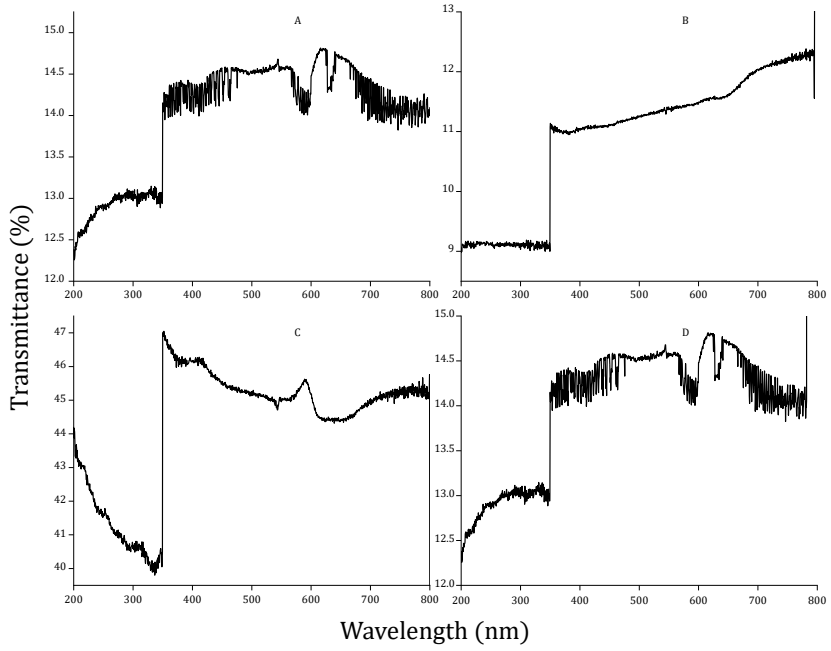

Fig. 9 Optical transmittance of ZnO NSs grown on WCF

vacancies. However in the case of Fig. 8(c), the graph indicates a dramatic drop in absorption value, followed by an increase, shortly after the 353 nm, which could be owing to the nanoflower shaped ZnO formed on WCF. As shown in Fig.9 and Fig.10, the transmittance and reflectance graphs of the grown ZnO NSs on WCF show irregular change of transmitted and reflected radiation near 350 nm. Due to morphological diversity of produced ZnO NSs on WCF, it can be assumed that the developed ZnO NSs have optical absorbance, optical transmittance, and optical reflectance up to a certain level in the visible range. The reflectance values of sample A, B, D are a combination of positive and negative value but sample C has positive values thus it can be concluded that only nanoflower shaped ZnO NSs have positive value of all three spectrums of UV-VIS spectroscopy.

3.3.1 Determination of the band gap value and Urbach energy

The energy band values (Eg) of the fabricated ZnO NSs on WCF samples were determined using following equation and Tauc's plot method (Al-Gaashani *et al.* 2013):

$$(\alpha h\upsilon)^n = B(h\upsilon - E_g) \tag{13}$$

where, α represents coefficient of absorption $h\upsilon$ represents photon energy, n represents the exponent of the band gap

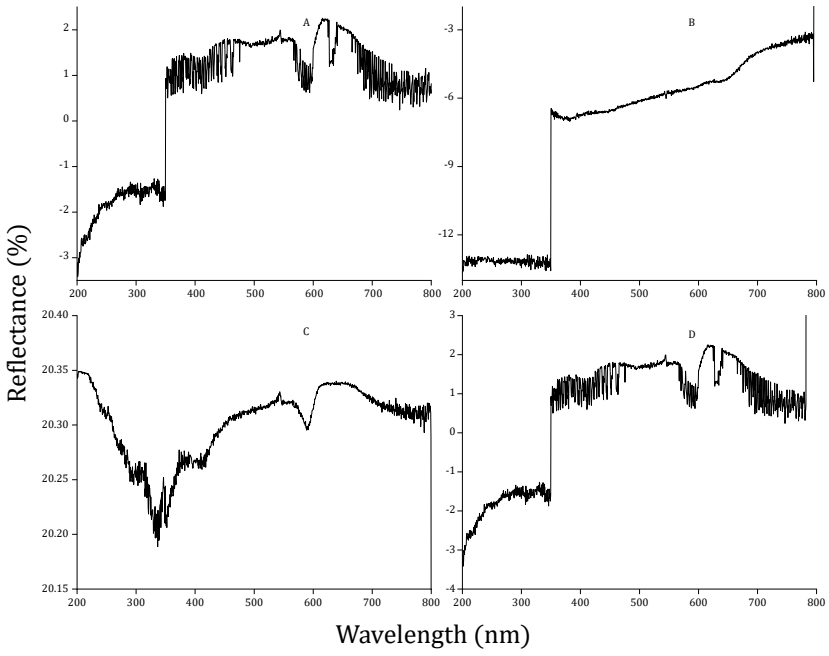

Fig. 10 Optical reflectance of ZnO NSs grown on WCF

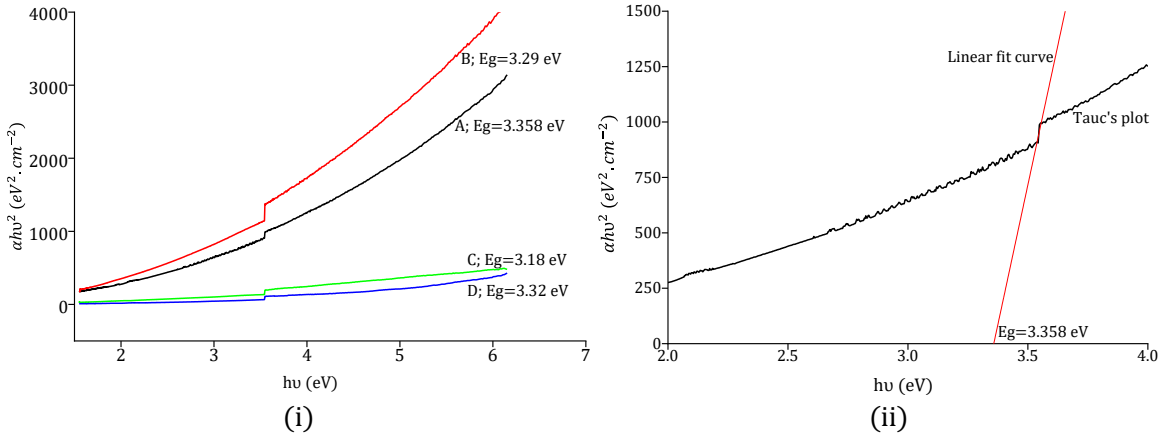

Fig. 11 (i) Tauc's plot of grown ZnO NSs and (b) Band gap calculation by linear fitting of Tauc's plot

which is ½ for indirect band and 2 for direct band. B is the constant depending upon material used. The value of α can be calculated by subsequent relation:

$$\alpha \approx \frac{2.303 \times A}{l} \tag{14}$$

where, A is absorbance value from UV-VIS spectra and L is the thickness of the film (in this case it is 4 μm). Tauc's plot is a plot between $(\alpha h\upsilon)^2$ and photon energy (hυ) as illustrated in the Fig. 11(i). As shown in Fig. 11(ii), the value of energy band gap for each sample can be determined by linear fitting analysis of their Tauc's plot. Table 2 displays the band gap values of various morphologies of ZnO on WCF. The computed energy gap is concordance with the energy gap of bulk ZnO (E_g=3.37 eV). Differing ZnO NSs morphologies exhibit different computed optical band gap values, in which ZnO nanopetals (sample-A) have higher value of band gap while ZnO nanoflowers (sample-C) possesses low band gap.

At the principal absorption line, the coefficient of absorption depends in exponential manner with the incident photon energy and compiles an empirical formula which is called Urbach's expression. Thus expression to calculate Urbach energy may be defined as (Caglar *et al.* 2009),

$$\alpha = \alpha_0 \exp\left[\frac{h\upsilon - E_1}{E_u}\right] \tag{15}$$

where, E_1 and α_0 represent constants and E_u represent Urbach energy which is equal to the width of the exponential absorption edge.

The Urbach energy E_u is a vital boundary to portray the problem of a material. It has to do with transitions between enlarged valence band circumstances and constrained conduction band ones. The width of the band's restricted states in the band gap is defined as the urbach energy, 'E_u'. It is possible to deduce the problem in the compound from the variation of the retention coefficient. The urbach energy 'E_u' represents the concept of material disorderliness and

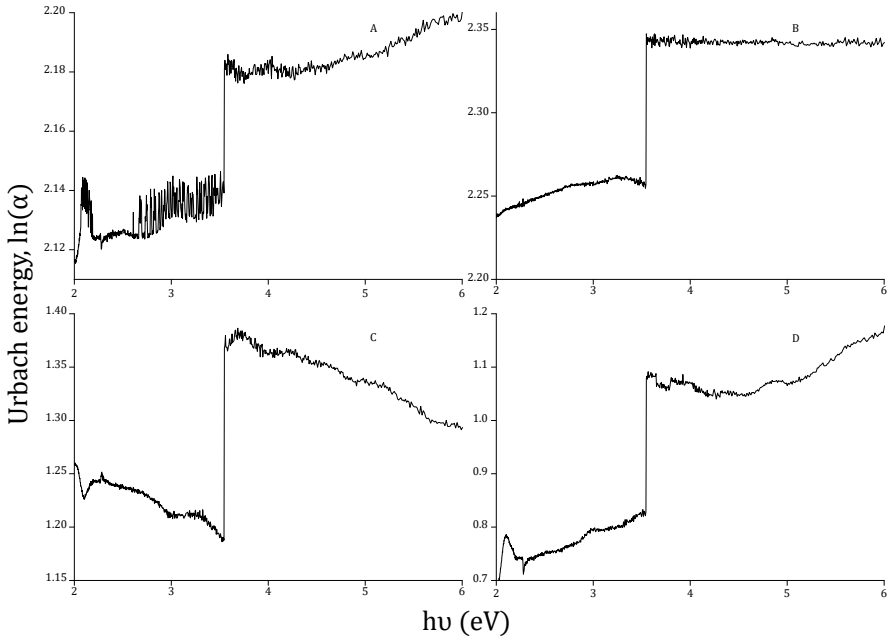

Fig. 12 Urbach energy of ZnO NSs grown on WCF

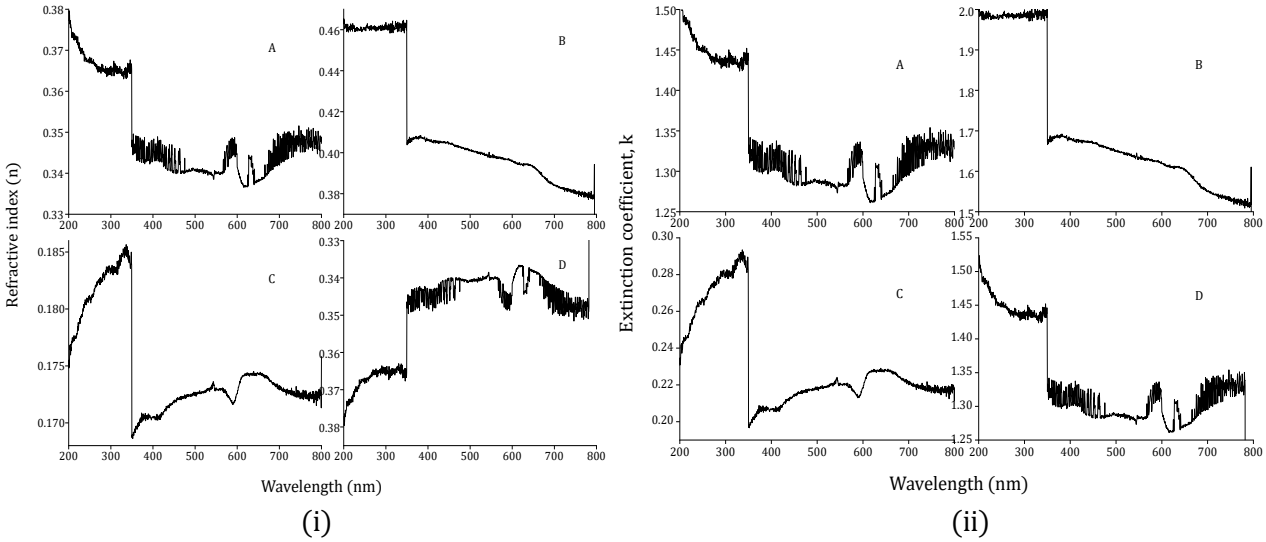

Fig. 13 Variation of (i) refractive index and (ii) extinction coefficient of grown ZnO NSs with wavelength

has been proven to be a crucial aspect in understanding material irregularity (Piccardo *et al.* 2017). It relates between expanded conditions of the valence band and confined condition of the conduction band. The urbach energy, 'E_u' is defined as the width of the confined state of the band gap. The change in the coefficient of absorption can be used to express disorder in a material. The plot against ln(α) and hυ of grown ZnO NSs on WCF reveals the amount of the urbach energy as illustrated in the Fig. 12. Samples A and D have growing urbach energies, whereas sample B has a stable value after ~3.6 eV photon energy, but sample C (nanoflowers) has started to decrease. This variation demonstrates the material's disorderliness, namely microstructural lattice disorder. The dependence of the optical coefficient of absorption with 'hυ' may appear from ambush levels at grain borders.

3.3.2 Study of refractive index and dielectric constants of grown ZnO NSs on WCF

The complicated behavior of refractive index and dielectric constants can also be used to define the optical properties of solid materials. Because dispersion is a vital parameter in optical communication and producing spectra dispersion appliances, dispersion plays an important role in the analysis of optical materials (Jia *et al.* 2022b). The optical performance of developed ZnO NSs in the UV-visible region was studied using absorbance, transmittance, and reflectance spectra. The refractive index is a function of wavelength n($\boldsymbol{\lambda}$) and can be derived from Fresnel's expression of reflectance as (Moss *et al.* 1974):

$$R = \frac{(n-1)^2 + k^2}{(n+1)^2 + k^2} \tag{16}$$

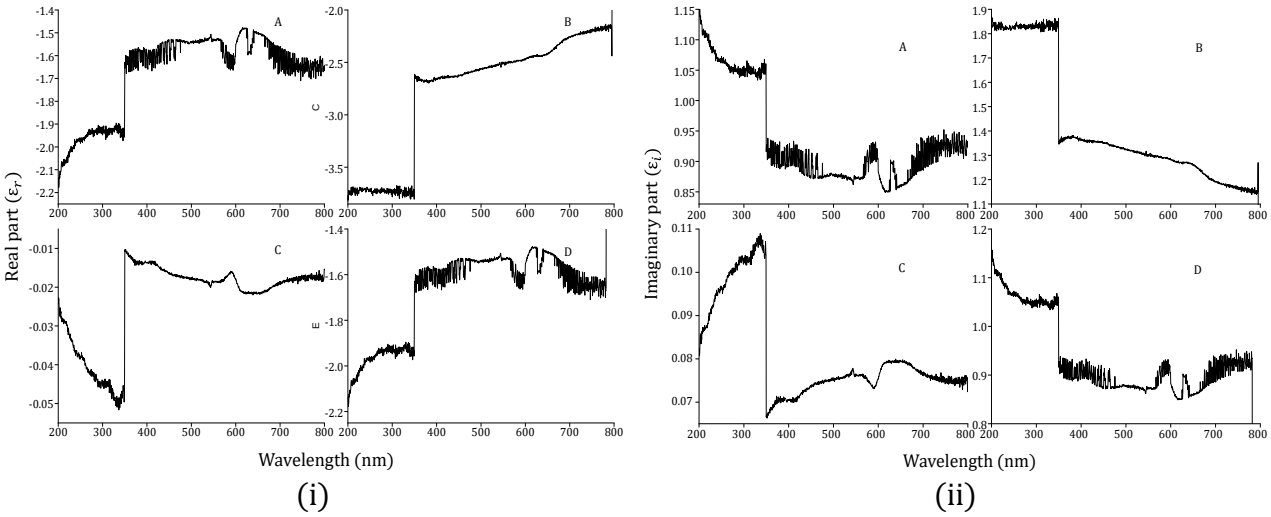

Fig. 14 Variation of (i) real part and (ii) imaginary part of dielectric function of ZnO NSs with wavelength

where, n and k represent factor of real and the imaginary portion of complex refractive index n*, and the factor $k = \frac{\alpha\lambda}{4\pi}$ is named as extinction coefficient. The expression of refractive index can be rewrite as (Moss *et al.* 1974):

$$n = \left(\frac{1+R}{1-R}\right) + \sqrt{\frac{4R}{(1-R)^2} - k^2} \tag{17}$$

The behavior of the observed refractive index with the function of wavelength is illustrated in Fig. 13(i). The graph reveals the non-monotonic variation of refractive index with respect to wavelength in the region of (200-360 nm) which is called "anomalous dispersion". The fluctuation then follows a normal dispersion pattern for the wavelength range (360-800 nm). The anomalous dispersion could be caused by a resonance between electromagnetic radiation and electron polarization, which causes electrons in ZnO NSs to pair with the oscillating electric field. Because of the growth of diverse morphologies of ZnO NSs on WCF surface, the refractive index of as grown ZnO NSs exhibit nonlinear and irregular variations for each sample, however there is a sudden change in the value of refractive index near the wavelength range of 350-360 nm. The variation of parameter $k = \frac{\alpha\lambda}{4\pi}$ (extinction coefficient) with the prescribed wavelength range in the visible region is illustrated in Fig. 13 (ii). Because of the nanoflowers shape of the ZnO, the values of 'k' for developed ZnO NSs decrease up to a particular wavelength range and subsequently increase for all samples except sample-C. The variation of 'k' for all samples is nonlinear and irregular and there is dramatic variation in the value near ~350-360 nm wavelengths due to different morphology of ZnO NSs. The frequency dependability of the complex dielectric function is used to characterize the principal electron excitation peak of ZnO NSs. It should also be mentioned that polarizability of solid is determined by their dielectric function, which is linked to the density of states in the forbidden band. As a result, understanding the nature of the real and imaginary parts of the dielectric function in terms of photon energy is critical. The complex dielectric function is expressed as (Liu *et al.* 2020),

$$\varepsilon^* = \varepsilon_r + i\varepsilon_i \tag{18}$$

where, ε_r and ε_i represents the real part and imaginary part of the dielectric function respectively. Also, ε_r and ε_i are depending on the n and k value in the subsequent manner:

$$\epsilon_r = n^2 - k^2 \text{ and } \epsilon_i = 2nk \tag{19}$$

The variation of ε_r and ε_i as a function of photon energy for the grown ZnO NSs on WCF is illustrated in Fig. 14(i) and Fig. 14(ii) respectively. The variation of dielectric constant of fabricated ZnO on WCF is nonlinear in the whole range of wavelengths but there is dramatic change in value near ~350-360 nm. It is caused because of the low estimation of the coefficient of extinction which is credited to the profound coefficient of absorption. Furthermore, the plot reveals that both ε_r and ε_i have non-monotonic changes, with ε_r being more articulated than ε_i. This pattern can be explained by the fact that in this energy range, specific collaborations between photons and electrons within the sample occur. The ε_r and ε_i of the dielectric function demonstrate almost similar model.

3.3.3 Optical conductivity

This is an important material feature that connects the current density to the electric field at normal frequencies. Optical conductivity is a modified kind of high-frequency electrical transfer. It is a contactless, quantitative test that's prone to charged outputs. The Optical conductivity of the material is computed from the following expression (Caglar *et al.* 2009):

$$\sigma_{opt.} = \frac{\alpha nc}{4\pi} \tag{20}$$

where α, n and c represent absorption coefficient, refractive index and speed of light (in vacuum) respectively. Fig. 15 illustrates the variation of optical conductivity of the synthesized ZnO NSs on WCF having different precursor

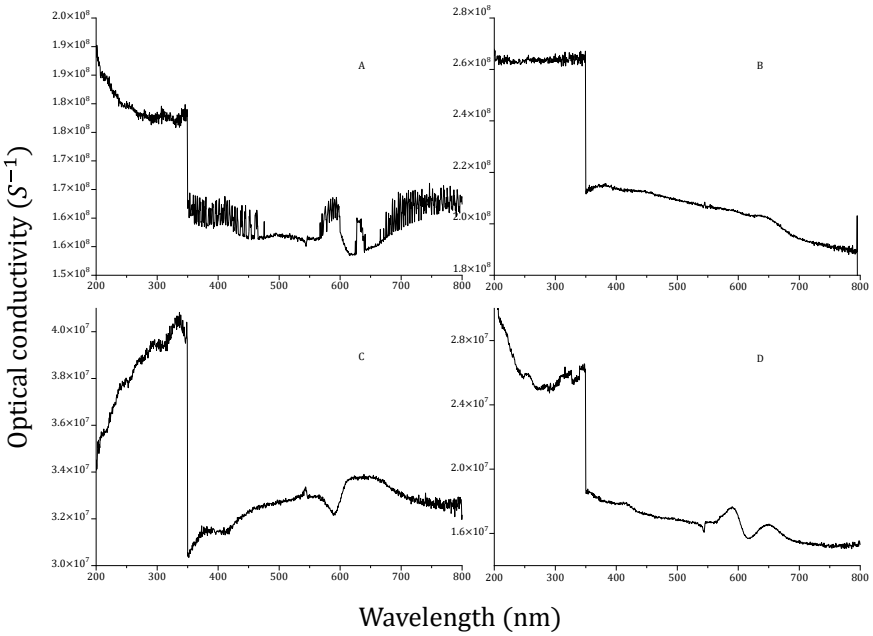

Fig. 15 Optical conductivity variation with wavelength for grown ZnO on WCF

solution treatment under microwave with in visible range. The plots of four different morphologies of ZnO reveal their particular conductivity nature. Because of the activation of electrons in interactions with photons, the behavior of optical conductivity (σ) with photon energy is nonlinear, as shown in the graph. The optical conductivity of nanoflowers (sample-C) displays a positive variation in conductivity value before ~353 nm wavelength, but then drops abruptly under the band gap region before increasing nonlinearly.

4. Future scope of ZnO NSs grown on WCF

Diverse utilities depending upon ZnO hierarchical structures are photocatalysis, active medium, field emission, sensors, water treatment, biomedical applications and electrodes (Ozdemira and Soyer 2021, Rai and Bajpai 2021b, Şahin and Kaya 2021). There are currently studies underway to incorporate the unique features of ZnO NSs into the field of high-performance composite materials. Due to increased mechanical qualities, particularly impact strength, some of the most prominent applications of such composites are in the aviation industry. Materials applications in robotics and artificial intelligence, sensors and biomaterials, microelectronics and photonics, and defense and artillery will all benefit from continuous advances in such materials. In comparison to natural carbon fibers, recent developments in the production of ZnO NSs on carbon fibers have led to a wide range of uses. Due to recent advancements in polymer-based nanocomposites, the use of nanocomposites in comparison to metals and ceramics is increasing due to their superior performance and characteristics (Deka *et al.* 2016, Forsat *et al.* 2021). As it can be clearly discovered, the prominent usages of nanocomposites are huge, consisting of evolution of advanced materials and the quality advancement of regarded components like sensors, cells and depositions (Bhammar *et al.* 2021, Shah and Rather, 2021). Still there is less application of nanocomposites in industries but advancements of these materials from research to industry is growing and in the coming few years it is expected to be extensive.

5. Conclusions

One step rapid growth of ZnO nanostructures on carbon fiber fabric using microwave-assisted chemical bath deposition technique has been advanced which is quicker than the chemical bath deposition process. Rapid heating of growth solution of $[Zn(NH_3)_4]^{2+}$ under microwave irradiation causes production of ZnO nanostructures by forced hydrolysis. The impact of different microwave synthesis parameters such as salt concentration, microwave duration and microwave power have great influence on morphologies and growth rates of the ZnO nanorods. The distributions and orientations of nanostructures can be optimized by tuning these process parameters and their reaction with growth solution. The impact of different kind of growth solution for the well distributed and uniform growth of ZnO nanostructures on carbon fiber fabric provides a basis to effective functionalization of fabrics. The FESEM result shows that nanostructures are irregular in shape and size but have smooth surface. The sizes of generated ZnO NSs were around 300-2300 nm in longitudinal direction and 200-1100 nm in lateral direction based on FESEM findings. The preferred orientation of ZnO growth is in the [1 0 1] direction, which is highest for nanoflowers, according to XRD and texture coefficient results. The optical characteristics of the samples reveal that nanopetals have a big band gap and nanoflowers have a small band gap which indicates greater size crystals possess smaller band gaps. The refractive index, extinction

coefficient, dielectric constant, Urbach energy, and optical conductivity of growing morphologies of ZnO on WCF surface are also investigated and depicted in graphs. The findings of all the analyses of grown ZnO NSs on WCF are in convergence with the already published experimental results and other available literatures. As formed ZnO NSs on WCF have these features, indicating that they have the potential to be employed in high performance nano-composites for optoelectronics and photonics applications such as sensors, emitters, catalysts, active medium, and electrodes. Its potential may be expanded in energy harvesting devices, bio-sensing, medicinal implementations, and environmental pollution sectors due to its outstanding morphological structure and enhanced surface to volume ratio.

Acknowledgement

Ravi Shankar Rai, Research Scholar, IIT-(ISM), Dhanbad, India, Dr. Vivek Bajpai, Assistant Professor, IIT-(ISM), Dhanbad, India have not been funded in any way to perform this research activities.

References

Ahmed, F., Arshi, N., Anwar, M.S., Danish, R. and Koo, B.H. (2014), "Morphological evolution of ZnO nanostructures and their aspect ratio-induced enhancement in photocatalytic properties", *RSC Adv.*, **4**(55), 29249-29263. https://doi.org/10.1039/C4RA02470B.

Al-Gaashani, R., Radiman, S., Daud, A.R., Tabet, N. and Al-Douri, Y. (2013), "XPS and optical studies of different morphologies of ZnO nanostructures prepared by microwave methods", *Ceram. Int.*, **39**(3), 2283-2292. https://doi.org/10.1016/j.ceramint.2012.08.075.

Alshamarti, H.A. and Omran Alkhayatt, A.H. (2020), "Enhancement characterization of the MSM detector based on Mn doped-ZnO NRS synthesized by microwave assisted chemical bath deposition", *Mater. Sci. Semiconduct. Proc.*, **114**, 105068. https://doi.org/10.1016/j.mssp.2020.105068.

Andrade Neto, N.F., Matsui, K.N., Paskocimas, C.A., Bomio, M.R.D. and Motta, F.V. (2019), "Study of the photocatalysis and increase of antimicrobial properties of Fe 3+ and Pb 2+ co-doped ZnO nanoparticles obtained by microwave-assisted hydrothermal method", *Mater. Sci. Semiconduct. Proc.*, **93**, 123-133. https://doi.org/10.1016/j.mssp.2018.12.034.

Arani, A.G., Farazin, A. and Mohammadimehr, M. (2021), "The effect of nanoparticles on enhancement of the specific mechanical properties of the composite structures: A review research", *Adv. Nano Res.*, **10**(4), 327-337. https://doi.org/10.12989/anr.2021.10.4.327.

Baizaee, S.M., Arabi, M. and Bahador, A.R. (2018), "A simple, one-pot, low temperature and pressure route for the synthesis of RGO/ZnO nanocomposite and investigating its photocatalytic activity", *Mater. Sci. Semiconduct. Proc.*, **82**, 135-142. https://doi.org/10.1016/j.mssp.2018.04.004.

Baruah, S. and Dutta, J. (2009), "Hydrothermal growth of ZnO nanostructures", *Sci. Technol. Adv. Mater.*, **10**, 013001. https://doi.org/10.1088/1468-6996/10/1/013001.

Bhammar, N.A., Udeshi, B., Dadhich, H., Dhokiya, V., Gadani, K., Venkateshwarlu, D., Venkatesh, R., Ganesan, V., Joshi, A.D., Solanki, P.S. and Shah, N.A. (2021), "Transport properties, charge conduction mechanism and magnetic behavior of La0.3Ca0.7MnO3:ZnO Nanocomposites", *Mater. Sci. Semiconduct. Proc.*, **135**, 106-130. https://doi.org/10.1016/j.mssp.2021.106130.

Caglar, M., Ilican, S., Caglar, Y. and Yakuphanoglu, F. (2009), "Electrical conductivity and optical properties of ZnO nanostructured thin film", *Appl. Surf. Sci.*, **255**(8), 4491-4496. https://doi.org/10.1016/j.apsusc.2008.11.055.

Caglar, Y., Gorgun, K. and Aksoy, S. (2015), "Effect of deposition parameters on the structural properties of ZnO nanopowders prepared by microwave-assisted hydrothermal synthesis", *Spectrochimica Acta A*, **138**, 617-622. https://doi.org/10.1016/j.saa.2014.12.008.

Chankaew, C., Tapala, W., Grudpan, K. and Rujiwatra, A. (2019), "Microwave synthesis of ZnO nanoparticles using longan seeds biowaste and their efficiencies in photocatalytic decolorization of organic dyes", *Environ. Sci. Pollut. Res.*, **26**(17), 17548-17554. https://doi.org/10.1007/s11356-019-05099-w.

Cheng, D., He, M., Li, W., Wu, J., Ran, J., Cai, G. and Wang, X. (2019), "Hydrothermal growing of cluster-like ZnO nano-particles without crystal seeding on PET films via dopamine anchor", *Appl. Surf. Sci.*, **467-468**, 534-542. https://doi.org/10.1016/j.apsusc.2018.10.177.

Cheng, Z., Song, H., Zhang, X., Cheng, X., Xu, Y., Zhao, H., Gao, S. and Huo, L. (2021), "Morphology control of ZnO by adjusting the solvent and non-enzymatic nitrite ions electro-chemical sensor constructed with stir bar-shaped ZnO/Nafion nanocomposite, *Sensors Actuat. B Chem.*, **346**, 130-525. https://doi.org/10.1016/j.snb.2021.130525.

Cortés Herrera, R.B., Kryshtab, T., Andraca Adame, J.A. and Kryvko, A. (2017), "ZnO thin films with Cu, Ga and Ag dopants prepared by ZnS oxidation in different ambient", *Adv. Nano Res.*, **5**(3), 193-201. https://doi.org/10.12989/anr.2017.5.3.193.

Deka, B.K., Hazarika, A., Kong, K., Kim, D., Park, Y. Bin, and Park, H.W. (2016), "Interfacial resistive heating and mechanical properties of graphene oxide assisted CuO nanoparticles in woven carbon fiber/polyester composite", *Compo. Part A Appl. Sci. Manuf.*, **80**, 159-170. https://doi.org/10.1016/j.compositesa.2015.10.023.

Deka, B.K., Hazarika, A., Kwon, O.B., Kim, D.Y., Park, Y.B, and Park, H.W. (2017), "Multifunctional enhancement of woven carbon fiber/ZnO nanotube-based structural supercapacitor and polyester resin-domain solid-polymer electrolytes", *Chem. Eng. J.*, **325**, 672-680. https://doi.org/10.1016/j.cej.2017.05.093.

Edalati, K., Shakiba, A., Vahdati-Khaki, J. and Zebarjad, S.M. (2016), "Low-temperature hydrothermal synthesis of ZnO nanorods: Effects of zinc salt concentration, various solvents and alkaline mineralizers", *Mater. Res. Bull.*, **74**, 374-379. https://doi.org/10.1016/j.materresbull.2015.11.001.

El-Nahas, S., El-sadek, M.S.A., Salman, H.M. and Elkady, M.M. (2021), "Controlled morphological and physical properties of ZnO nanostructures synthesized by domestic microwave route", *Mater. Chem. Phys.*, **258**, 123-885. https://doi.org/10.1016/j.matchemphys.2020.123885.

Feng, T., Liu, N., Wang, S., Qin, C., Shi, S., Zeng, X. and Liu, G. (2021), "Research on the dispersion of carbon nanotubes and their application in solution-processed polymeric matrix composites: A review", *Adv. Nano Res.*, **10**(6), 559-576. https://doi.org/10.12989/anr.2021.10.6.545.

Forsat, M., Musharavati, F., Eltai, E., Zain, A.M., Mobayen, S. and Mohamed, A.M. (2021), "Vibration characteristics of microplates with GNPs-reinforced epoxy core bonded to piezoelectric-reinforced CNTs patches", *Adv. Nano Res.*, **11**(2), 115-140. https://doi.org/10.12989/anr.2021.11.2.115.

Ganesan, V., Hariram, M., Vivekanandhan, S. and Muthuramkumar, S. (2020), "Periconium sp. (endophytic fungi)

extract mediated sol-gel synthesis of ZnO nanoparticles for antimicrobial and antioxidant applications", *Mater. Sci. Semiconduct. Proc.*, **105**, 104-739. https://doi.org/10.1016/j.mssp.2019.104739.

Gusmao, L.A., Peixoto, D.A., Marinho, J.Z., Romeiro, F.C., Gonçalves, R.F., Longo, E., de Oliveira, C.A. and Lima, R.C. (2021), "Alkali influence on ZnO and Ag-doped ZnO nanostructures formation using the microwave-assisted hydrothermal method for fungicidal inhibition", *J. Phys. Chem. Solids*, **158**, 110-234. https://doi.org/10.1016/j.jpcs.2021.110234.

Hazarika, A., Deka, B.K., Kim, D. Y., Kong, K., Park, Y. Bin, and Park, H.W. (2015), "Growth of aligned ZnO nanorods on woven Kevlar® fiber and its performance in woven Kevlar® fiber/ polyester composites", *Compos. Part A*, **78**, 284-293. https://doi.org/10.1016/j.compositesa.2015.08.022.

Jia, Z., Kong, M., Yu, B., Ma, Y., Pan, J. and Wu, G. (2022), "Tunable Co/ZnO/C@ MWCNTs based on carbon nanotube-coated MOF with excellent microwave absorption properties", *J. Mater. Sci. Technol*., **127**, 153-163. https://doi.org/10.1016/j.jmst.2022.04.005.

Jia, Z., Liu, X., Zhou, X., Zhou, Z. and Wu, G. (2022), "A seed germination-inspired interface polarization augmentation strategy toward superior electromagnetic absorption performance", *Compos. Commun*., **34**, 101269. https://doi.org/10.1016/j.coco.2022.101269.

Kim, S.O., Shim, J.B. and Chang, H. (2011), "Rapid hydrothermal synthesis of zinc oxide nanowires by annealing methods on seed layers", *J. Nanomater*., **2011**, 582764. https://doi.org/10.1155/2011/582764.

Kong, K., Deka, B.K., Kwak, S.K., Oh, A., Kim, H., Park, Y.B., and Park, H.W. (2013), "Processing and mechanical characterization of ZnO/polyester woven carbon-fiber composites with different ZnO concentrations", *Compos. Part A*, **55**, 152-160. https://doi.org/10.1016/j.compositesa.2013.08.013.

Kothari, A. and Chaudhuri, T.K. (2011), "One-minute microwave-assisted chemical bath deposition of nanostructured ZnO rod-arrays", *Mater. Lett*., **65**(5), 847-849. https://doi.org/10.1016/j.matlet.2010.12.017.

Kumar, D., Rai, R.S., and Singh, N.K. (2020), "An innovative approach to deposit ultrathin ZnO nanoflakes (2D) through hydrothermal assisted electrochemical discharge deposition and growth method", *Ceram. Int*., **46**(16), 26216-26220. https://doi.org/10.1016/j.ceramint.2020.07.009.

Kumar, V.V.S. and Kanjilal, D. (2018), "Influence of post-deposition annealing on structural, optical and transport properties of nanocomposite ZnO-Ag thin films", *Mater. Sci. Semiconduct. Proc.*, **81**, 22-29. https://doi.org/10.1016/j.mssp.2018.03.002.

Kurtinaitiene, M., Mazeika, K., Ramanavicius, S., Pakstas, V. and Jagminas, A. (2016), "Effect of additives on the hydrothermal synthesis of manganese ferrite nanoparticles", *Adv. Nano Res*., **4**(1), 1-14. https://doi.org/10.12989/anr.2016.4.1.001.

Liu, Z., Li, L., Yuan, X. and Yang, P. (2020), "Study on photoelectric properties of Si supported ZnO", *J. Alloys Compd*., **843**, 155909. https://doi.org/10.1016/j.jallcom.2020.155909.

Liu, Y., Jia, Z., Zhou, J. and Wu, G. (2022), "Multi-hierarchy heterostructure assembling on MnO2 nanowires for optimized electromagnetic response", *Mater. Today Phys*., **28**, 100845. https://doi.org/10.1016/j.mtphys.2022.100845.

Liu, J., Jia, Z., Dong, Y., Li, J., Cao, X. and Wu, G. (2022), "Structural engineering and compositional manipulation for high-efficiency electromagnetic microwave absorption", *Mater. Today Phys*., **27**, 100801. https://doi.org/10.1016/j.mtphys.2022.100801.

Ma, J., Chen, B., Chen, B., and Zhang, S. (2017), "Preparation of superparamagnetic ZnFe2O4 submicrospheres via a solvothermal method", *Adv. Nano Res*., **5**(2), 171-178. https://doi.org/10.12989/anr.2017.5.2.171.

Mallakpour, S., Sirous, F. and Hussain, C.M. (2021), "A journey to the world of fascinating ZnO nanocomposites made of chitosan, starch, cellulose, and other biopolymers: Progress in recent achievements in eco-friendly food packaging, biomedical, and water remediation technologies", *Int. J. Biol. Macromol.*, **170**, 701-716. https://doi.org/10.1016/j.ijbiomac.2020.12.163.

Marin-Flores, C.A., Rodriguez-Nava, O., Garcia-Hernandez, M., Ruiz-Guerrero, R., Juarez-Lopez, F. and Morales-Ramirez, A.J. (2021), "Free-radical scavenging activity properties of ZnO sub-micron particles: size effect and kinetics", *J. Mater. Res. Technol*., **13**, 1665-1675. https://doi.org/10.1016/j.jmrt.2021.05.050.

Moss, T.S., Burrell, G.J., Ellis, B., and Omar, M.A. (1974), "Semiconductor opto-electronics", *Phys. Today*, **27**(2), 59. https://doi.org/10.1063/1.3128454.

Newcomb, B.A. (2016), "Processing, structure, and properties of carbon fibers", *Compos. Part A*, **91**(1), 262-282. https://doi.org/10.1016/j.compositesa.2016.10.018.

Ozdemira, O.O. and Soyer, F. (2021), "Synthesis, characterization, and antimicrobial activities of 3-HPAA-Alg-Chi nanoparticles", *Adv. Nano Res*., **11**(3), 227-237. https://doi.org/10.12989/anr.2021.11.3.227.

Patino-Portela, M.C., Arciniegas-Grijalba, P.A., Mosquera-Sanchez, L.P., Sierra, B.E.G., Munoz-Florez, J.E., Erazo-Castillo, L.A. and Rodriguez-Paez, J.E. (2021), "Effect of method of synthesis on antifungal ability of ZnO nanoparticles: Chemical route vs green route", *Adv. Nano Res*., **10**(2), 191-210. https://doi.org/10.12989/anr.2021.10.2.191.

Piccardo, M., Li, C.K., Wu, Y.R., Speck, J.S., Bonef, B., Farrell, R.M., Filoche, M., Martinelli, L., Peretti, J. and Weisbuch, C. (2017), "Localization landscape theory of disorder in semiconductors. II. Urbach tails of disordered quantum well layers", *Phys. Rev. B*, **95**(14), 144-205. https://doi.org/10.1103/PhysRevB.95.144205.

Radhakrishnan, J.K. and Kumara, M. (2021), "Growth of ZnO nanostructures: Cones, rods and hallow-rods, by microwave assisted wet chemical growth and their characterization", *Ceram. Int*., **47**(4), 5300-5310. https://doi.org/10.1016/j.ceramint.2020.10.110.

Rai, R.S. and Bajpai, V. (2021a), "Hydrothermally grown ZnO NSs on Bi-Directional woven carbon fiber and effect of synthesis parameters on morphology", *Ceram. Int*., **47**(6), 8208-8217. https://doi.org/10.1016/j.ceramint.2020.11.180.

Rai, R.S. and Bajpai, V. (2021b), "Recent advances in ZnO nanostructures and their future perspective", *Adv. Nano Res*., **11**(1), 37-54. https://doi.org/10.12989/anr.2021.11.1.037.

Sahin, B. and Kaya, T. (2021), "Facile preparation and characterization of nanostructured ZnO/CuO composite thin film for sweat concentration sensing applications", *Mater. Sci. Semiconduct. Proc*., **121**, 105428. https://doi.org/10.1016/j.mssp.2020.105428.

Shah, A.H. and Rather, M.A. (2021), "Pharmaceutical residues: New emerging contaminants and their mitigation by nano-photocatalysis", *Adv. Nano Res*., **10**(4), 397-414. https://doi.org/10.12989/anr.2021.10.4.397.

Singh, P.P. and Azam, M.S. (2021), "Size dependent vibration of embedded functionally graded nanoplate in hygrothermal environment by Rayleigh-Ritz method", *Adv. Nano Res*., **10**(1), 25-42. https://doi.org/10.12989/anr.2021.10.1.025.

Ul Hassan Sarwar Rana, A., Kang, M. and Kim, H.S. (2016), "Microwave-assisted facile and ultrafast growth of ZnO nanostructures and proposition of alternative microwave-assisted methods to address growth stoppage", *Sci. Rep*., **6**(24870), 1-13. https://doi.org/10.1038/srep24870.

Wang, Y., Yang, J., Li, Y., Jiang, T., Chen, J. and Wang, J. (2015), "Controllable preparation of ZnO nanostructure using hydrothermal-electrodeposited method and its properties", *Mater. Chem. Phys.*, **153**, 266-273. https://doi.org/10.1016/j.matchemphys.2015.01.013.

Zhang, Z.Y. and Xiong, H.M. (2015), "Photoluminescent ZnO nanoparticles and their biological applications", *Materials*, **8**(6), 3101-3127. https://doi.org/10.3390/ma8063101.

Zhao, Z., Liu, W., Jiang, Y., Wan, Y., Du, R. and Li, H. (2022), "Solidification of heavy metals in lead smelting slag and development of cementitious materials", *J. Clean. Prod.*, **359**, 132134. https://doi.org/10.1016/j.jclepro.2022.132134.

CC